fractal and fractional

Article

Swarm Intelligence Procedures Using Meyer Wavelets as a Neural Network for the Novel Fractional Order Pantograph Singular System

Zulqurnain Sabir [1], Muhammad Asif Zahoor Raja [2], Juan L. G. Guirao [3,4,*] and Tareq Saeed [4]

[1] Department of Mathematics and Statistics, Hazara University, Mansehra 21300, Pakistan; zulqurnain_maths@hu.edu.pk
[2] Future Technology Research Center, National Yunlin University of Science and Technology, 123 University Road, Section 3, Douliu 64002, Yunlin County, Taiwan; rajamaz@yuntech.edu.tw
[3] Department of Applied Mathematics and Statistics, Technical University of Cartagena, Hospital de Marina, 30203 Cartagena, Spain
[4] Nonlinear Analysis and Applied Mathematics (NAAM)-Research Group, Department of Mathematics, Faculty of Science, King Abdulaziz University, P.O. Box 80203, Jeddah 21589, Saudi Arabia; tsalmalki@kau.edu.sa
* Correspondence: juan.garcia@upct.es or jlgarcia@kau.edu.sa

Abstract: The purpose of the current investigation is to find the numerical solutions of the novel fractional order pantograph singular system (FOPSS) using the applications of Meyer wavelets as a neural network. The FOPSS is presented using the standard form of the Lane–Emden equation and the detailed discussions of the singularity, shape factor terms along with the fractional order forms. The numerical discussions of the FOPSS are described based on the fractional Meyer wavelets (FMWs) as a neural network (NN) with the optimization procedures of global/local search procedures of particle swarm optimization (PSO) and interior-point algorithm (IPA), i.e., FMWs-NN-PSOIPA. The FMWs-NN strength is pragmatic and forms a merit function based on the differential system and the initial conditions of the FOPSS. The merit function is optimized, using the integrated capability of PSOIPA. The perfection, verification and substantiation of the FOPSS using the FMWs is pragmatic for three cases through relative investigations from the true results in terms of stability and convergence. Additionally, the statics' descriptions further authorize the presentation of the FMWs-NN-PSOIPA in terms of reliability and accuracy.

Keywords: fractional order pantograph singular system; Meyer wavelets; shape factors; neural networks; interior point; particle swarm optimization

Citation: Sabir, Z.; Raja, M.A.Z.; Guirao, J.L.G.; Saeed, T. Swarm Intelligence Procedures Using Meyer Wavelets as a Neural Network for the Novel Fractional Order Pantograph Singular System. *Fractal Fract.* **2021**, *5*, 277. https://doi.org/10.3390/fractalfract5040277

Academic Editor: Ivanka Stamova

Received: 4 November 2021
Accepted: 5 December 2021
Published: 17 December 2021

1. Introduction

The differential systems signified with fractional and integer orders are used extensively in several applications of physics, engineering and mathematics. Fractional calculus operators (FCOs) have been famous for scientists during the last three to four decades [1]. Some noteworthy applications of the FCOs are Weyl–Riesz [2], Grnwald–Letnikov [3], Riemann–Liouville [4] and Erdlyi–Kober [5]. Many scientists have described the importance of FCOs in diverse areas of fractional viscoplasticity models [6], Earth-based dynamical investigations [7], reaction networks of surface–volume [8], electromagnetic studies [9], detection of road edges [10], comprehensive performances in authentic supplies [11], mathematical nanofluids [12], viscoelastic systems [13] and LC-electric fractal circuit systems [14].

It is always considered tough to solve singular models with the use of numerical or analytical approaches. Singular models arise in spherical surfaces of gas clouds, astrophysics studies and quantum mechanics and are always considered difficult for researchers due to the harder nature and the occurrence of singular points. A variety of deterministic schemes have been executed to solve singular based models [15–18]. The literature form of the singular second-order system is described as [19–21]:

$$\begin{cases} \frac{d^2k}{d\eta^2} + \frac{\gamma}{\eta}\frac{dk}{d\eta} + g(k) = h(\eta), \quad \gamma \geq 1 \\ k(0) = i_1,\ k'(0) = i_2, \end{cases} \tag{1}$$

where γ represents the shape vector value in Equation (1), the singularity arises at $\eta = 0$, $h(\eta)$ is the forcing term and $g(k)$ is some known function of k, while i_1 and i_2 are the constants representing the initial conditions.

The differential form of the pantographs is a specific state of the functional model that contains proportional delay factors. Tayler and Ockendon introduced the "pantograph" word in the 7th decade of the 19th century by working on the collection of the pantograph electric head [22]. The pantograph differential system (PDS) has achieved huge importance due to its well-known applications in the biological system of cell growth [23], asymptotic constancy characteristics [24] and control networks [25]. A number of approaches have been applied to solve singular models, e.g., the Chebyshev spectral method [26], spectral tau technique [27], intricate homotopy optimal method [28], Genocchi scheme of operation matrix [29], Epsilon–Ritz-based least-square approach [30] and Taylor method [31]. The novelty of this study is described in two steps as follows:

1. The design of a novel fractional order pantograph singular system (FOPSS) is presented using the suitable derivation process.
2. The computing process based on machine learning or soft computing knacks is implemented to solve the novel FOPSS using the applications of the Meyer wavelets based fractional neural network.

The current investigations are relevant to design a novel FOPSS using the applications of Meyer wavelets as a neural network by implementing the concepts of the traditional singular second-order differential equation and pantograph differential model [32]. The numerical discussions of the FOPSS are provided based on the fractional Meyer wavelets (FMWs) as a neural network (NN) with the optimization procedures of global/local search procedures of particle swarm optimization (PSO) and interior-point algorithm (IPA), i.e., FMWs-NN-PSOIPA. The stochastic schemes based on numerical measures is applied to solve a variety of applications [33–40], and a few potential recently reported applications include the solution of nonlinear Lane–Emden multi-pantograph delay based ordinary differential equations (ODEs) [41], Gudermannian neural networks for sODEs [42], neuro-swarming approach to singular with multiple delay ODEss [43], intelligent backpropagated networks for solving Lene–Emden singular ordinary differential systems with pantograph delays [44], novel design of Morlet wavelet neural networks for solving singular pantograph nonlinear differential models [45], third kind of multi-singular nonlinear systems [46], novel design of evolutionary integrated heuristics for singular systems [47], Morlet wavelet neural networks for solving higher order singular nonlinear ODEs [48] and wavelet analysis on some surfaces of revolution [49]. All these applications inspire the authors to investigate the design of FOPSS, which has never been implemented nor treated, by using the proposed heuristics of FMWs-NN-PSOIPA.

FMWS-NN-PSOIPA is implemented to solve the novel FOPSS using the applications of Meyer wavelets as neural networks. The FOPSS is stiff in nature, involving singular points, pantographs and fractional order nature. A few novel features of the FMWs-NN-PSOIPA are provided as follows:

- A novel FOPSS is presented using the pantograph differential system (PDS) and fundamental form of the second-order singular model.
- The numerical performance of the novel FOPSS is obtained by using the designed approach FMWs-NN-PSOIPA, which is used to compare the obtained results and to perform the values of the absolute error (AE).
- The Meyer computing solvers via FMWs-NN-PSOIPA is applied to solve three examples based on the novel FOPSS to authenticate the convergence, precision and stability.

- The reliability of the proposed FMWS-NN-PSOIPA is accessible using the statistical procedures in terms of semi-interquartile range (S.I.R), Theil's inequality coefficient (T.I.C) and variance account for (VAF).

Alongside the precise performance of the novel FOPSS, its easy understandable process, smooth operations, steadiness and sturdiness are other valued compensations of the fractional Meyer intelligent computing solver.

The other paper parts are presented as follows: Section 2 represents the design of the novel FOPSS using the applications of Meyer wavelets as a neural network. Section 3 presents the proposed procedure using the FMWs-NN-PSOIPA. Section 4 indicates the statistical performance. Section 5 defines the concluding remarks and future research reports.

2. Construction of the Novel FOPSS

This part of the study shows the construction of the novel FOPSS along with the comprehensive details of the shape factor (SF), singular point and fractional order factor. The necessary procedural steps to construct the novel FOPSS are drawn on the flow chart, while the construction of the novel FOPSS is provided as:

$$\eta^{-p}\frac{d^r}{d\eta^r}\left(\eta^p\frac{d^u}{d\eta^u}\right)k\left(\frac{\eta}{2}\right)+g(k)=h(\eta), \tag{2}$$

For the novel FOPSS, the values of p and r are provided as follows:

$$r=1,\ \ u=\Re,\text{ where } 0<\Re<1. \tag{3}$$

The restructured form for the above two systems is given as:

$$\eta^{-p}\frac{d}{d\eta}\left(\eta^p\frac{d^{\Re}}{d\eta^{\Re}}\right)k\left(\frac{\eta}{2}\right)+g(k)=h(\eta). \tag{4}$$

The simplification of Equation (4) is written as:

$$\frac{d}{d\eta}\left(\eta^p\frac{d^{\Re}}{d\eta^{\Re}}\right)k\left(\frac{\eta}{2}\right)=\eta^p\frac{d^{\Re+1}}{d\eta^{\Re+1}}k\left(\frac{\eta}{2}\right)+p\eta^{p-1}\frac{d^{\Re}}{d\eta^{\Re}}k\left(\frac{\eta}{2}\right). \tag{5}$$

The achieved form of the novel FOPSS is provided as:

$$\begin{cases}\frac{d^{\Re+1}}{d\eta^{\Re+1}}k\left(\frac{\eta}{2}\right)+\frac{p}{\eta}\frac{d^{\Re}}{d\eta^{\Re}}k\left(\frac{\eta}{2}\right)+g(k)=h(\eta),\\ k(0)=0,\quad k(1)=0.\end{cases} \tag{6}$$

The novel FOPSS is achieved above in Equation (6) with the singular point occurring at $\eta=0$; The fractional terms are noticed as $\Re$ and $\Re+1$, respectively, whereas the SF is at $p=1$. The flow chart based on the novel FOPSS describing the essential phases is provided in the block structure in Figure 1. These procedures are used to design a novel FOPSS system described in terms of mathematical relation given in Equations (2)–(6).

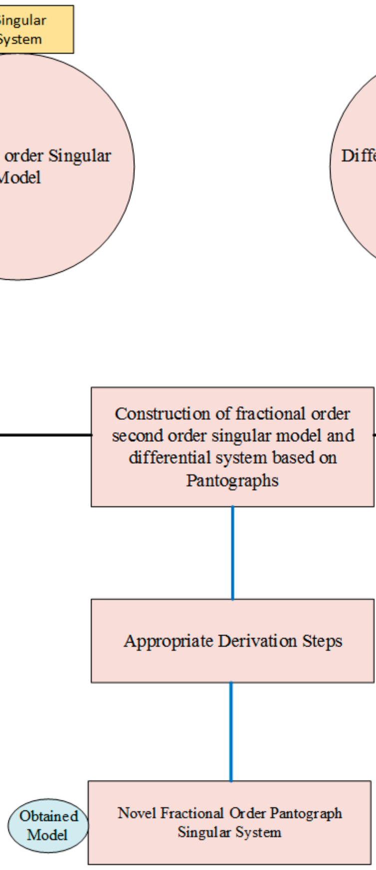

Figure 1. Flow-chart diagram using the essential steps of the novel FOPSS.

3. Methodology: FMWs-NN-PSOIPA

This section shows the proposed methodology using the FMWs as a NN along with the optimal methods of PSOIPA for solving the novel FOPSS. The process flow diagram of FMWs-NN-PSOIPA is portrayed in Figure 2 in terms of five blocks for the problem, modeling, learning, storage and results. The error function is constructed using the differential form and boundary conditions (BCs) together with the optimization procedure of PSOIPA provided here.

3.1. Objective Function: FMWs-NN

The ANNs systems are familiar to obtain the numerical performances of numerous systems based on the fractional order [42,43]. In the below system, $\hat{k}(\eta)$ is the proposed solution form of the network, $D^{(n)}\hat{k}(\eta)$ and $D^{\Re}\hat{k}(\eta)$ indicate the nth order derivative and the fractional order form, respectively. These systems' terminologies take the following forms:

$$\begin{aligned} \hat{k}(\eta) &= \sum_{m=1}^{z} r_m p(c_m\eta + b_m), \\ D^{(n)}\hat{k}(\eta) &= \sum_{m=1}^{z} r_m p^{(n)}(c_m\eta + b_m), \\ D^{\Re}\hat{k}(\eta) &= \sum_{m=1}^{z} r_m p^{\Re}(c_m\eta + b_m) \end{aligned} \tag{7}$$

where z represents the neurons. Similarly, $\boldsymbol{r}$, $\boldsymbol{c}$ and $\boldsymbol{b}$ represent the components of weight vector ($\boldsymbol{W}$), shown as:

$$\boldsymbol{W} = [\boldsymbol{r}, \boldsymbol{c}, \boldsymbol{b}], \text{ for } \boldsymbol{r} = [r_1, r_2, \ldots, r_z], \quad c = [c_1, c_2, \ldots, c_z] \text{ and } \boldsymbol{b} = [b_1, b_2, \ldots, b_z] .$$

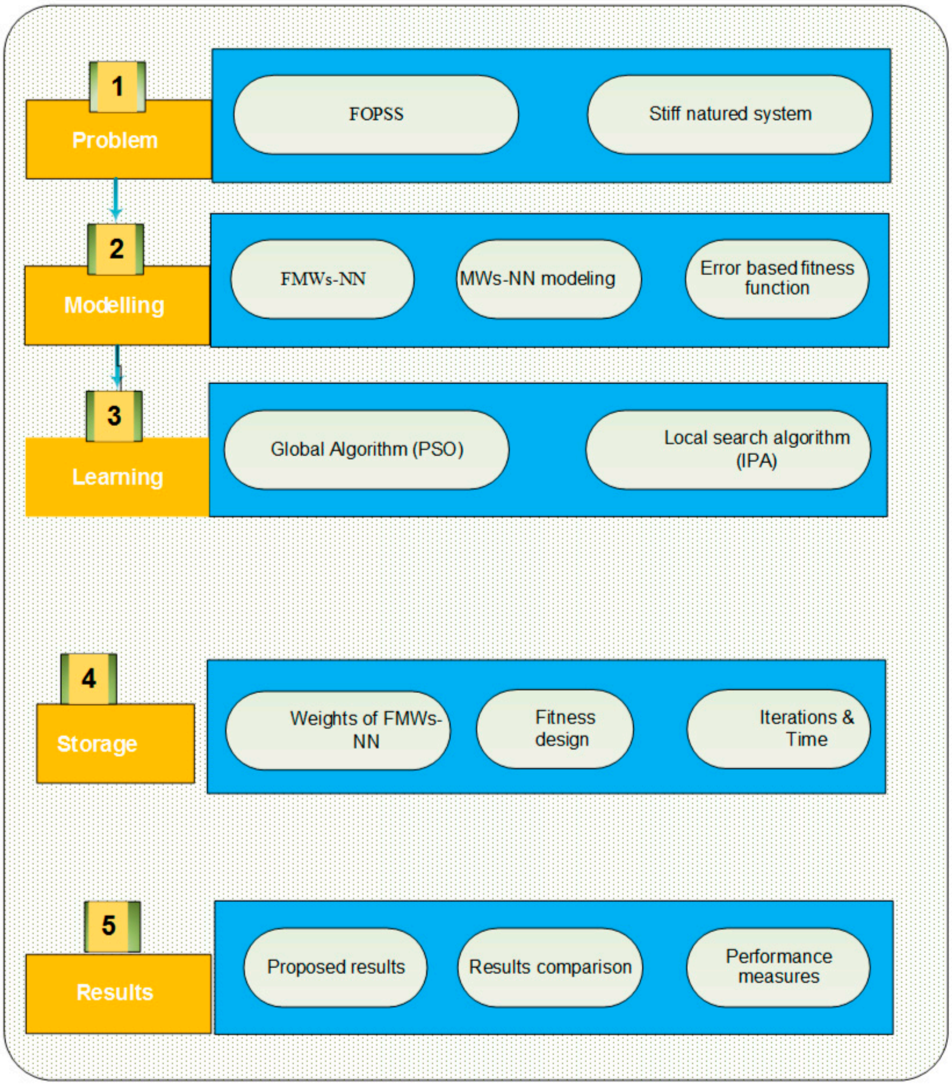

Figure 2. Design procedures of the FMWs-NN-PSOIPA for solving the novel FOPSS.

The mathematical representations the activation kernel based on the Meyer wavelet function is shown as:

$$p(\eta) = 35\eta^4 - 84\eta^5 + 70\eta^6 - 20\eta^7. \tag{8}$$

The combination of the network (7) and (8) becomes:

$$\begin{aligned} \hat{k}(\eta) &= \sum_{m=1}^{z} r_m \begin{pmatrix} 35(c_m\eta + b_m)^4 - 84(c_m\eta + b_m)^5 + \\ 70(c_m\eta + b_m)^6 - 20(c_m\eta + b_m)^7 \end{pmatrix}, \\ D^{(n)}\hat{k}(\eta) &= \sum_{m=1}^{z} r_m \begin{pmatrix} 35D^{(\mathrm{n})}(c_m\eta + b_m)^4 - 84D^{(\mathrm{n})}(c_m\eta + b_m)^5 \\ +70D^{(\mathrm{n})}(c_m\eta + b_m)^6 - 20D^{(\mathrm{n})}(c_m\eta + b_m)^7 \end{pmatrix}, \\ D^{\Re}\hat{k}(\eta) &= \sum_{m=1}^{z} r_m \begin{pmatrix} 35D^{\Re}(c_m\eta + b_m)^4 - 84D^{\Re}(c_m\eta + b_m)^5 + \\ 70D^{\Re}(c_m\eta + b_m)^6 - 20D^{\Re}(c_m\eta + b_m)^7 \end{pmatrix}. \end{aligned} \tag{9}$$

The procedures of the arbitrary FMWs-NN are implemented for the novel FOPSS associated to the obtainability of suitable W. To assess the weights of FMWs-NN, one may calculate the theory of approximation with the mean squared error terminology to find an error function ε_{Fit}, given as:

$$\varepsilon_{Fit} = \varepsilon_{Fit-1} + \varepsilon_{Fit-2}. \tag{10}$$

where ε_{Fit-1} and ε_{Fit-2} are the error functions related to the differential system and its BCs, shown as:

$$\varepsilon_{Fit-1} = \frac{1}{N}\sum_{m=1}^{z}\left(\frac{d^{\Re+1}}{d\eta^{\Re+1}}\hat{k}_m + \frac{p}{\eta_m}\frac{d^{\Re}}{d\eta^{\Re}}\hat{k}_m + g(\hat{k}_m) - h_m\right)^2, \tag{11}$$

$$\varepsilon_{Fit-2} = \frac{1}{2}\left(\left(\hat{k}_0\right)^2 + \left(\hat{k}_N\right)^2\right), \tag{12}$$

for $Nh = 1,\ \hat{k}_m = \hat{k}\left(\frac{\eta_m}{2}\right),\ h_m = h(\eta_m),\ \eta_m = mh.$

3.2. Optimization of the Network

In this section, the parameter optimization procedures for the FMWs-NN are considered using the computing constructions of PSOIPA for solving the novel FOPSS.

Particle swarm optimization is a global search approach implemented to solve optimization problems. It is applied as an alternate of the genetic algorithm approach introduced at the end of the 19th century. PSO is a nature-based metaheuristic due to its immense optimization abilities in the large search spans. PSO executes efficiently as compared to the genetic algorithm due to its small amount of memory. In the process of PSO, the primary swarm escalates in the substantial domain. For the PSO improvement, the procedure produces iteratively optimal outcomes $\boldsymbol{P}_{LB}^{h-1}$ for swarm's position and $\boldsymbol{P}_{GB}^{h-1}$ for swarm's velocity, given as:

$$\boldsymbol{X}_i^h = \boldsymbol{X}_i^{h-1} + \boldsymbol{V}_i^{h-1}, \tag{13}$$

$$\begin{aligned}\boldsymbol{V}_i^h = \Re\boldsymbol{V}_i^{h-1} + h_1(\boldsymbol{P}_{LB}^{h-1} - \boldsymbol{X}_i^{h-1})\boldsymbol{r}_1 \\ +h_2(\boldsymbol{P}_{GB}^{h-1} - \boldsymbol{X}_i^{h-1})\boldsymbol{r}_2,\end{aligned} \tag{14}$$

where the inertia vector based on weight is $\Re$, the position is $\boldsymbol{X}_i$ and the velocity is $\boldsymbol{V_i}$, while, h_1 and h_2 are acceleration constant factors. A few prominent applications of the PSO are optimal reactive power dispatch [50], fusion of features for detection of brain tumor [51], energy-efficient routing mechanism for mobile sink in wireless sensor networks [52], optimal power flow problems [53], dynamic service composition focusing on quality-of-service evaluations under hybrid networks [54] and enhancing the production of biodiesel from Microalga [55].

The convergence of the PSO scheme is more reliable using the hybridization process with the local search *interior-point algorithm*, which is used to find the fine-tuning of the outcomes. IPA is a valued approach, which is used to confine the system for improved understanding together with the optimization procedures of the designed system. In recent decades, IPA has been applied in optimal operation of interconnected energy hubs [56], economic load dispatch [57], a nonlinear well-determined model for power system observability [58] and power control of multiple interfering D2D communications underlaying cellular networks [59].

3.3. Performance Indices

In this work, the mathematical formulations of the performances based on the TIC, ENSE and EVAF along with the global illustrations of these indices to solve the novel FOPSS are provided as:

$$\begin{cases}\text{VAF} = \left(1 - \frac{\text{var}\left(k_j - \hat{k}_j\right)}{\text{var}\left(k_j\right)}\right) \times 100, \\ \text{EVAF} = |VAF - 100|.\end{cases} \tag{15}$$

$$\text{T.I.C} = \frac{\sqrt{\frac{1}{n}\sum_{j=1}^{q}\left(k_j - \hat{k}_j\right)^2}}{\left(\sqrt{\frac{1}{n}\sum_{j=1}^{q}k_j^2} + \sqrt{\frac{1}{n}\sum_{j=1}^{q}\hat{k}_j^2}\right)}, \tag{16}$$

$$\begin{cases} \text{NSE} = \begin{cases} 1 - \dfrac{\sum_{j=1}^{q}\left(k_j - \hat{k}_j\right)^2}{\sum_{j=1}^{q}\left(k_j - \bar{k}_j\right)^2}, & \bar{k}_j = \frac{1}{n}\sum_{j=1}^{q} k_j \end{cases} \\ ENSE = 1 - NSE, \end{cases} \tag{17}$$

where $\hat{k}$ and k are the proposed and exact solutions. The necessary comparison of the proposed FMWs-NN-PSOIPA is conducted with respect to magnitudes of VAF, TIC and NSE for perfect modeling scenarios with values 100, 0 and 1, respectively.

4. Simulations and Results

In this section, the numerical implementations to solve three examples of the novel FOPSS are provided. The proposed outcomes along FMWs-NN-PSOIPA that depend upon 40 executions to solve the novel FOPSS are provided with essential graphical and numerical depictions to evaluate the accurateness and convergence.

Suppose a novel FOPSS is shown as:

$$\begin{cases} \eta \frac{d^{\Re+1}}{d\eta^{\Re+1}} k\left(\frac{\eta}{2}\right) + \frac{d^{\Re}}{d\eta^{\Re}} k\left(\frac{\eta}{2}\right) + \eta g(k) = \eta h(\eta) = F(\eta), \\ k(0) = k(1) = 0, \end{cases} \tag{18}$$

where

$$\begin{gathered} F(\eta) = \eta\left(\frac{\sqrt{(1+w)}}{\sqrt{1-\Re+w}}\left(\frac{\eta}{2}\right)^{w-\Re} - \frac{\sqrt{1+y}}{\sqrt{1-\Re+y}}\left(\frac{\eta}{2}\right)^{z-\Re} \right) \\ + \frac{\sqrt{w+1}}{\sqrt{w-\Re+1}}\left(\frac{\eta}{2}\right)^{w-\Re} - \frac{\sqrt{1+y}}{\sqrt{1-\Re+y}}\left(\frac{\eta}{2}\right)^{z-\Re} + \eta^{w+1} - \eta^{y+1} \end{gathered} \tag{19}$$

where w and y are selected as positive. The modernized form using the above equations is given as:

$$\begin{cases} \eta \frac{d^{\Re+1}}{d\eta^{\Re+1}} k\left(\frac{\eta}{2}\right) + \frac{d^{\Re}}{d\eta^{\Re}} k\left(\frac{\eta}{2}\right) + \eta h(k) = \eta \left(\begin{array}{c} \frac{\sqrt{(1+w)}}{\sqrt{1-\Re+w}}\left(\frac{\eta}{2}\right)^{w-\Re} \\ -\frac{\sqrt{1+y}}{\sqrt{1-\Re+y}}\left(\frac{\eta}{2}\right)^{z-\Re} \end{array} \right) \\ + \frac{\sqrt{w+1}}{\sqrt{w-\Re+1}}\left(\frac{\eta}{2}\right)^{w-\Re} - \frac{\sqrt{1+y}}{\sqrt{1-\Re+y}}\left(\frac{\eta}{2}\right)^{z-\Re} + \eta^{w+1} - \eta^{y+1}, \\ k(0) = k(1) = 0. \end{cases} \tag{20}$$

The true solution is given as:

$$k(\eta) = \eta^{w} - \eta^{y} \tag{21}$$

For the specific performances of w = 3 and y = 2, the true solution is accomplished as:

$$k(\eta) = \eta^3 - \eta^2. \tag{22}$$

An error function is given as:

$$\begin{gathered} \varepsilon_{Fit} = \frac{1}{N}\sum_{m=1}^{z} \left(\begin{array}{l} \eta_m \frac{d^{\Re+1}}{d\eta_m^{\Re+1}} \hat{k}\left(\frac{\eta_m}{2}\right) + \frac{d^{\Re}}{d\eta_m^{\Re}} \hat{k}\left(\frac{\eta_m}{2}\right) + \eta_m h(\hat{k}_m) \\ -\eta_m^{w+1} + \eta_m^{z+1} - \eta_m \sqrt{\frac{w+1}{w-\Re+1}} \left(\frac{\eta_m}{2}\right)^{w-\Re} \\ +\eta_m \sqrt{\frac{y+1}{y-\Re+1}} \left(\frac{\eta_m}{2}\right)^{y-\Re} - \sqrt{\frac{w+1}{w-\Re+1}} \left(\frac{\eta_m}{2}\right)^{w-\Re} \\ +\sqrt{\frac{y+1}{y-\Re+1}} \left(\frac{\eta_m}{2}\right)^{y-\Re} \end{array} \right)^2 \\ +\frac{1}{2}\left(\left(\hat{k}_0\right)^2 + \left(\hat{k}_N\right)^2 \right). \end{gathered} \tag{23}$$

Three different types of the novel FOPSS are provided using the α values, respectively given as $\alpha = 0.2, 0.4$ and 0.6.

In order to examine the performance of each type of novel FOPSS, optimization is performed using the local and global search techniques, i.e., PSOIPA. The entire procedure is repeated for 40 independent runs to create a larger dataset of the parameters of FMWs-NN. These trained FMWs-NN weights are given in Equation (9) to evaluate the outcomes of the novel FOPSS. The mathematical form of the FMWs-NN-PSOIPA for each type of novel FOPSS is provided as:

$$\begin{aligned}\hat{k}_{E-1} = -0.113&\begin{pmatrix} 35(-0.971\eta+0.570)^4 - 84(-0.971\eta+0.5708)^5 \\ +70(-0.971\eta+0.5708)^6 - 20(-0.971\eta+0.5708)^7 \end{pmatrix} \\ +0.3448&\begin{pmatrix} 35(0.0641\eta+1.0772)^4 - 84(0.0641\eta+1.0772)^5 \\ +70(0.0641\eta+1.0772)^6 - 20(0.0641\eta+1.0772)^7 \end{pmatrix} + \cdots \\ +0.0267&\begin{pmatrix} 35(0.2990\eta+1.2633)^4 - 84(0.2990\eta+1.2633)^5 \\ +70(0.2990\eta+1.2633)^6 - 20(0.2990\eta+1.2633)^7 \end{pmatrix},\end{aligned} \tag{24}$$

$$\begin{aligned}\hat{k}_{E-2} = -0.426&\begin{pmatrix} 35(0.430\eta-0.4234)^4 - 84(0.4300\eta-0.4234)^5 \\ +70(0.4300\eta-0.4234)^6 - 20(0.4300\eta-0.4234)^7 \end{pmatrix} \\ +2.1279&\begin{pmatrix} 35(-0.117\eta-0.028)^4 - 84(-0.117\eta-0.0284)^5 \\ +70(-0.117\eta-0.0284)^6 - 20(-0.117\eta-0.0284)^7 \end{pmatrix} + \cdots \\ -0.5029&\begin{pmatrix} 35(0.950\eta-0.2247)^4 - 84(0.95000\eta-0.2247)^5 \\ +70(0.9500\eta-0.2247)^6 - 20(0.9500\eta-0.2247)^7 \end{pmatrix},\end{aligned} \tag{25}$$

$$\begin{aligned}\hat{k}_{E-3} = -0.2573&\begin{pmatrix} 35(0.304\eta-0.2064)^4 - 84(0.3041\eta-0.2064)^5 \\ +70(0.3041\eta-0.2064)^6 - 20(0.3041\eta-0.2064)^7 \end{pmatrix} \\ -0.1217&\begin{pmatrix} 35(0.0244\eta+1.3782)^4 - 84(0.0244\eta+1.3782)^5 \\ +70(0.0244\eta+1.3782)^6 - 20(0.0244\eta+1.3782)^7 \end{pmatrix} + \cdots \\ +0.406&\begin{pmatrix} 35(-0.2985\eta-0.046)^4 - 84(-0.5903\eta-0.5980)^5 \\ +70(-0.5903\eta-0.598)^6 - 20(-0.590\eta-0.598)^7 \end{pmatrix}.\end{aligned} \tag{26}$$

The estimated results through the FMWs-NN are indicated in systems (24)–(26) with the graphical plots illustrated in Figure 3a–c for each class of novel FOPSS. The mean, best and worst results comparison is drawn in Figure 3d–f for each class of novel FOPSS. It is observed that these outcomes are matched to each other. This accuracy of the numerical results shows the quality of the designed FMWs-NN-PSOIPA. The AE performance is obtained in Figure 3g for each class of novel FOPSS. It is observed that the performance of AE is calculated around 10^{-1} to 10^{-3}, 10^{-2} to 10^{-3} and 10^{-1} to 10^{-3} for Examples 1, 2 and 3, respectively. The convergence is assessed using the FIT, ENSE, TIC and EVAF measures, drawn in Figure 3h for each class of novel FOPSS. It is indicated that the best performance instances of the FIT measure are found around 10^{-5}–10^{-6}, 10^{-4}–10^{-5} and 10^{-3}–10^{-5} for each example of the novel FOPSS. The EVAF performance instances are calculated around 10^{-4} to 10^{-5} for each example of the novel FOPSS. The TIC measures' performance instances are calculated around 10^{-3} to 10^{-5} for each example of the novel FOPSS. The ENSE is calculated around 10^{-4} to 10^{-5} for each variant of the novel FOPSS.

The TIC, ENSE, FIT and EVAF performance instances with the histogram and boxplots are drawn in Figures 4–7 for each class of the novel FOPSS. It is demonstrated that the FIT performance is calculated around 10^{-3} to 10^{-6}, 10^{-4} to 10^{-5} and 10^{-3} to 10^{-5} for Examples 1, 2 and 3. TIC lies around 10^{-3} to 10^{-5} for Example 1, whereas the other two examples of TIC values are found around 10^{-3} to 10^{-5}. The EVAF and ENSE values for each case of the novel FOPSS lie in the ranges of 10^{-1} to 10^{-2} and 10^{-2} to 10^{-3}, respectively. These best measures, calculated through statistical gages, authenticate the correctness of FMWs-NN-PSOIPA.

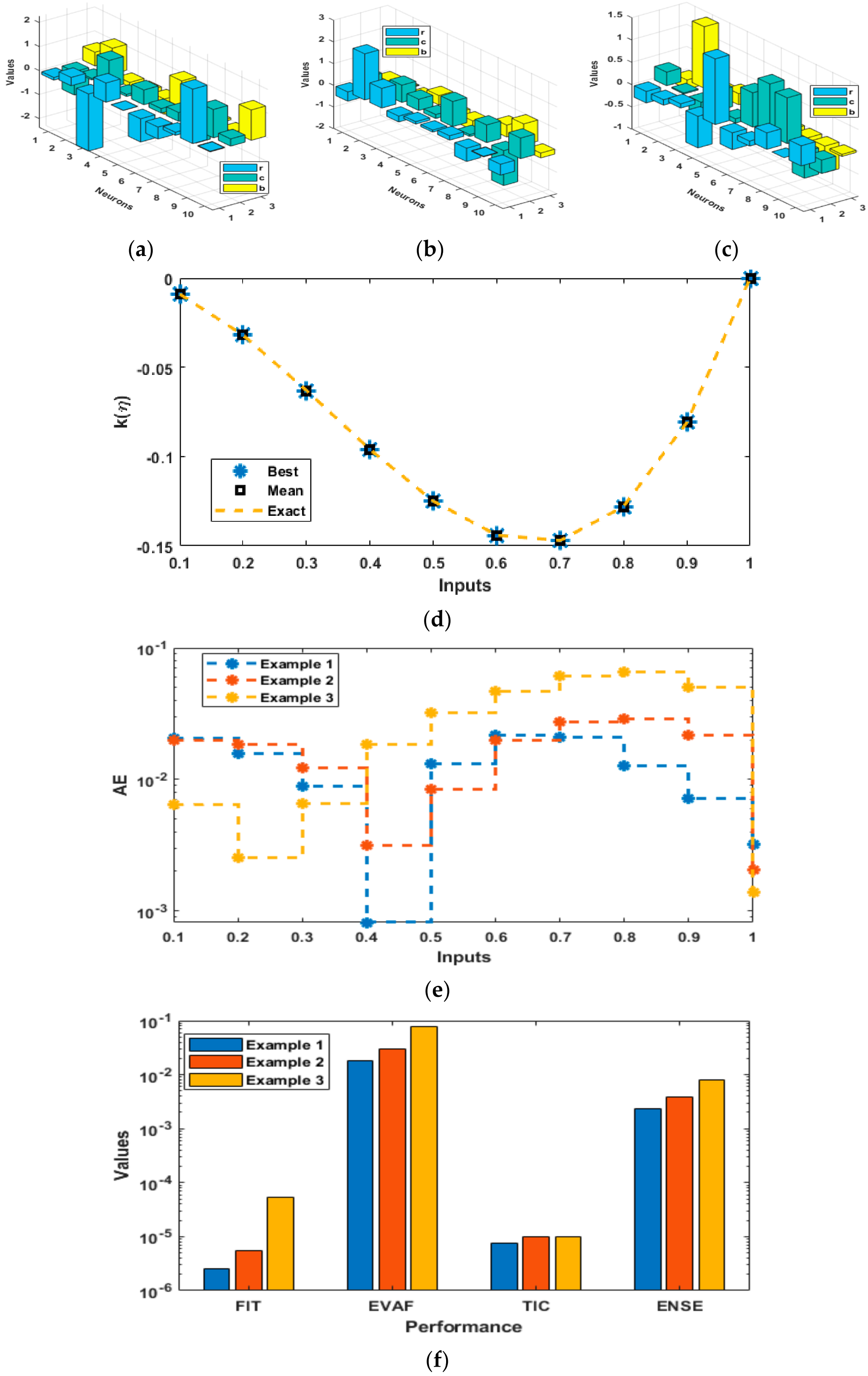

Figure 3. Graphical illustrations are provided in (**a**–**c**), best weights in (**d**–**f**), AE in (**e**) and performance in (**f**) for solving the novel FOPSS. (**a**) Best weights, Example 1; (**b**) best weights, Example 2; (**c**) best weights, Example 3; (**d**) FOPSS results for Examples 1, 2 and 3; ((**e**) AE performance instances for each class of the novel FOPSS; (**f**) performance instances for each example of the novel FOPSS.

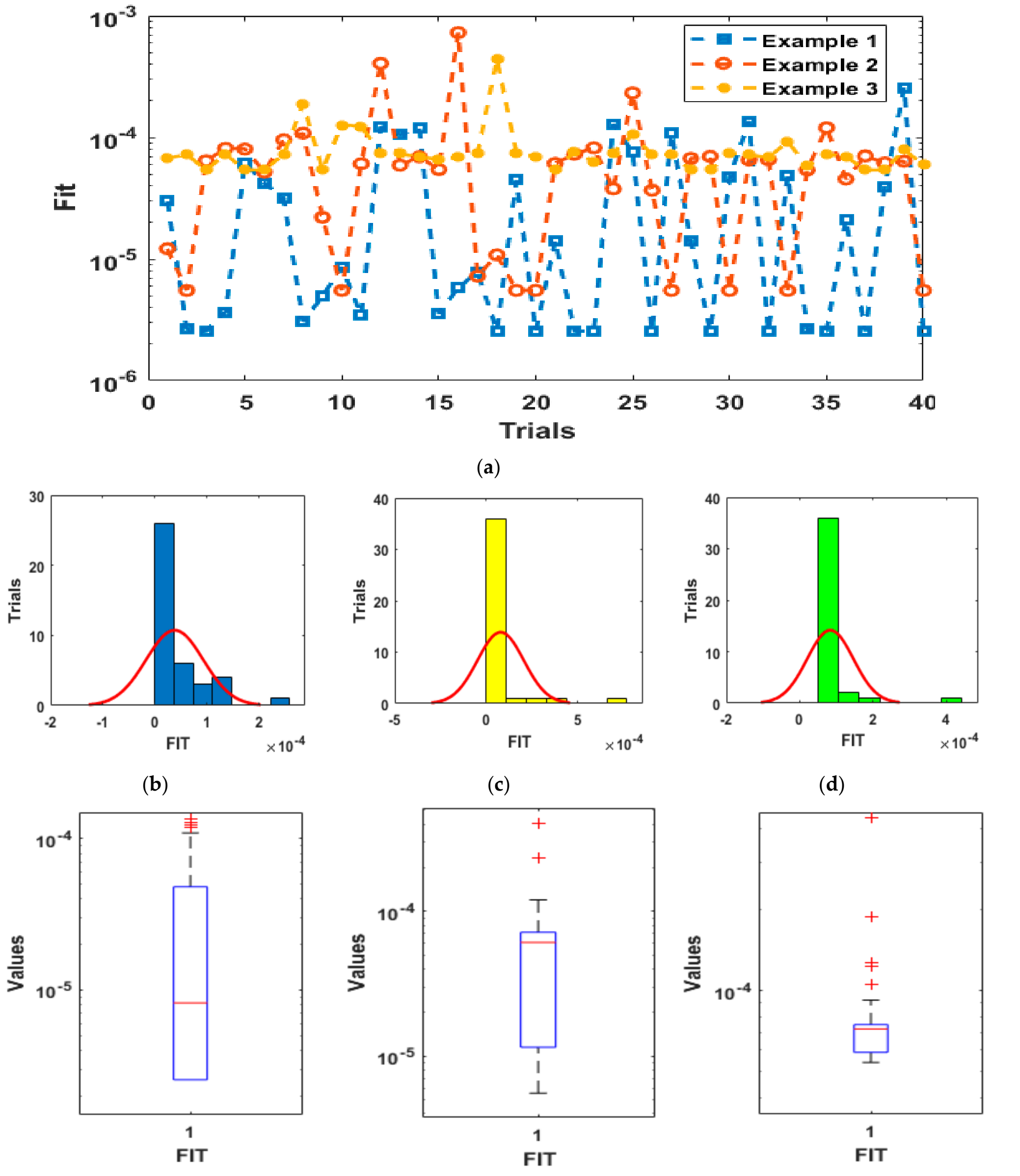

(**a**)

(**b**) (**c**) (**d**)

(**e**) (**f**) (**g**)

Figure 4. Statistics values through FMWs-NN-PSOIPA for FIT performance with histogram/boxplots for the novel FOPSS. (**a**) FIT investigations for each example; (**b**) histograms for 1st example; (**c**) histograms for 2nd example; (**d**) histograms for 3rd example; (**e**) boxplots for 1st example; (**f**) boxplots for 2nd example; and (**g**) boxplots for 3rd example.

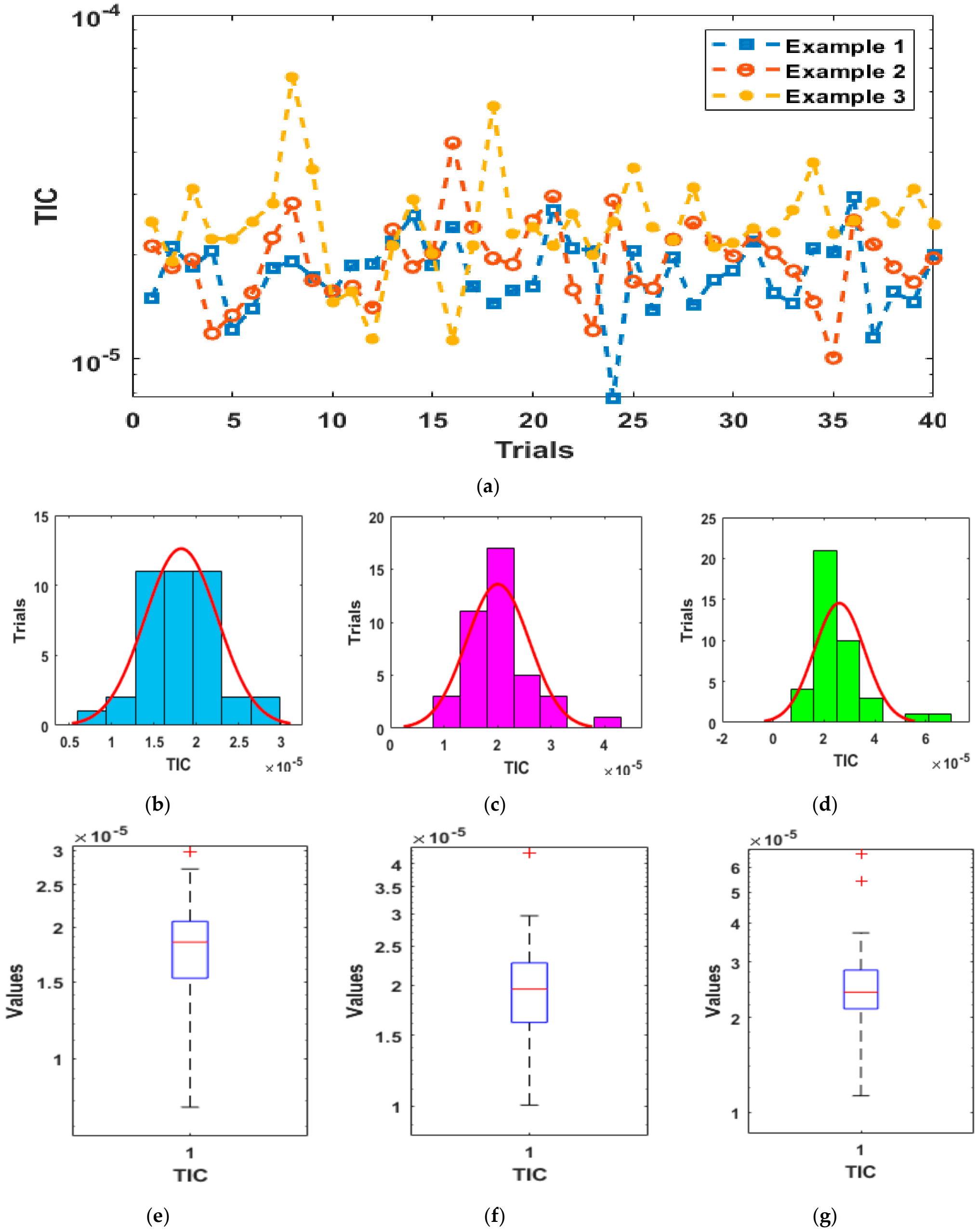

Figure 5. Statistics values through FMWs-NN-PSOIPA for TIC performance with histogram/boxplots for the novel FOPSS. (**a**) TIC investigations for each example; (**b**) histograms for 1st example; (**c**) histograms for 2nd example; (**d**) histograms for 3rd example; (**e**) boxplots for 1st example; (**f**) boxplots for 2nd example; and (**g**) boxplots for 3rd example.

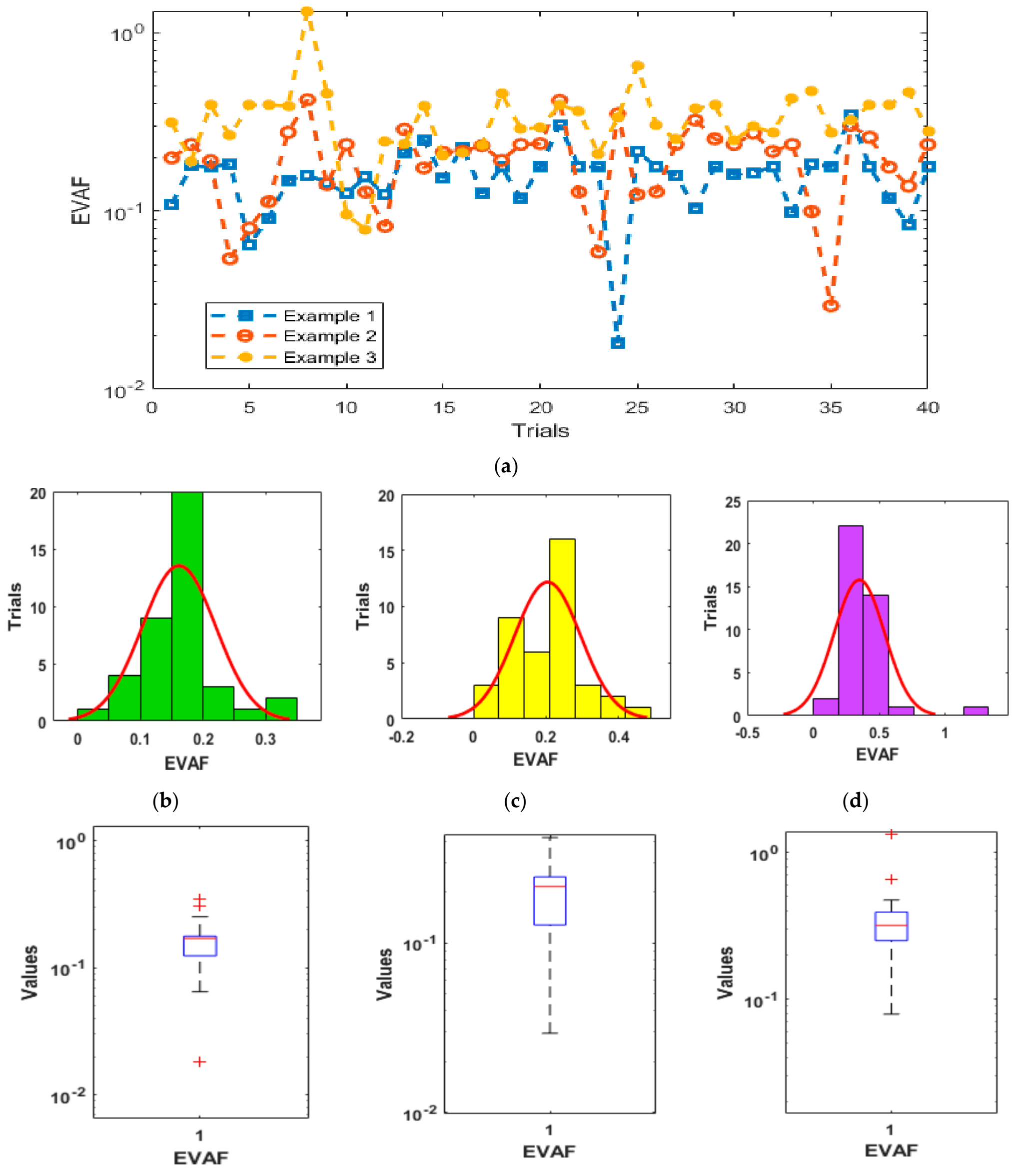

(**a**)

(**b**) (**c**) (**d**)

(**e**) (**f**) (**g**)

Figure 6. Statistics values through FMWs-NN-PSOIPA for EVAF performance with histogram/boxplots for the novel FOPSS. (**a**) EVAF investigations for each example; (**b**) histograms for 1st example; (**c**) histograms for 2nd example; (**d**) histograms for 3rd example; (**e**) boxplots for 1st example; (**f**) boxplots for 2nd example; and (**g**) boxplots for 3rd example.

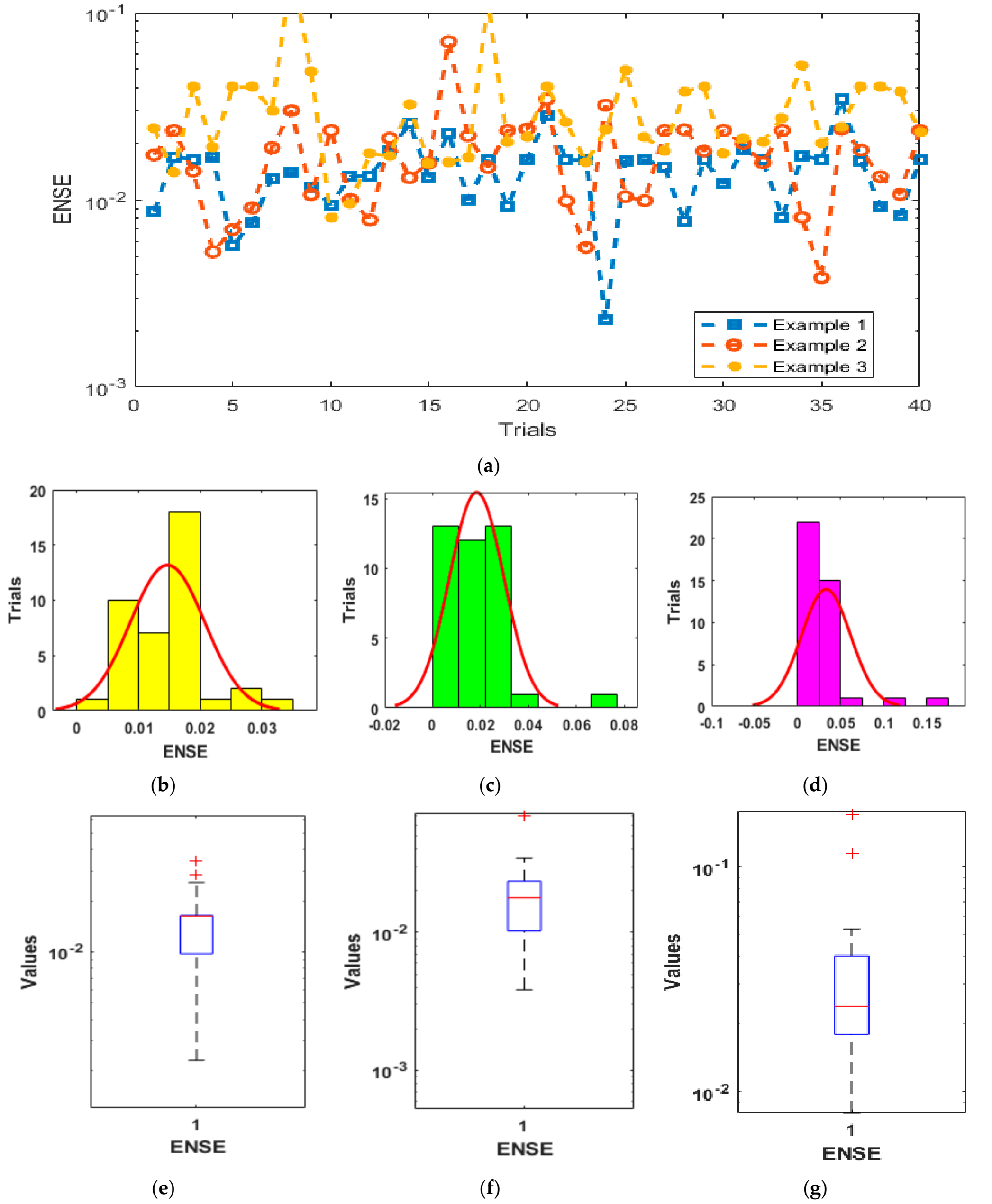

Figure 7. Statistics values through FMWs-NN-PSOIPA for ENSE performance with histogram/boxplots for the novel FOPSS. (**a**) ENSE investigations for each example; (**b**) histograms for 1st example; (**c**) histograms for 2nd example; (**d**) histograms for 3rd example; (**e**) boxplots for 1st example; (**f**) boxplots for 2nd example; and (**g**) boxplots for 3rd example.

In order to check the precision and exactness, the statistical measures, through standard deviation (STD), minimum (Min), S.I.R, mean, maximum (Max) and median (MED), are found for 40 accomplishments of FMWs-NN-PSOIPA as shown in Table 1 for solving the novel FOPSS. The Max and Min values indicate the worst and best executions, while S.I.R represents one half of the 3rd minus 1st quartiles. The values based on Min, Max, MED, Mean, S.I.R and S.T.D for Example 1 are found around 10^{-3}–10^{-5}, 10^{-2}–10^{-3}, 10^{-2}–10^{-3}, 10^{-2}–10^{-4}, 10^{-2}–10^{-3} and 10^{-3}–10^{-5}. In Example 2, the performance lies around 10^{-2}–10^{-6}, 10^{-1}–10^{-2}, 10^{-2}–10^{-4}, 10^{-2}–10^{-3}, 10^{-2}–10^{-3} and 10^{-2}–10^{-4}. Likewise, in Example 3, the performance lies around 10^{-3} to 10^{-5}, 10^{-1} to 10^{-3}, 10^{-2} to 10^{-3}, 10^{-2} to 10^{-3}, 10^{-2} to 10^{-3} and 10^{-2} to 10^{-5}. These calculated consistent and small performance instances of each operative authenticate the accuracy and constancy of FMWs-NN-PSOIPA for solving the novel FOPSS.

Table 1. Statistics illustrations through FMWs-NN-PSOIPA for solving the novel FOPSS.

Index	Mode	Proposed Outcomes $k(\eta)$									
		0.1	0.2	0.3	0.4	0.5	0.6	0.7	0.8	0.9	1
1	Min	4×10^{-4}	3×10^{-4}	1×10^{-3}	8×10^{-4}	4×10^{-3}	4×10^{-4}	1×10^{-3}	1×10^{-2}	3×10^{-3}	3×10^{-5}
	Max	4×10^{-2}	3×10^{-2}	3×10^{-2}	3×10^{-2}	4×10^{-2}	6×10^{-2}	8×10^{-2}	9×10^{-2}	7×10^{-2}	5×10^{-3}
	MED	6×10^{-3}	1×10^{-2}	1×10^{-2}	2×10^{-2}	3×10^{-2}	4×10^{-2}	5×10^{-2}	5×10^{-2}	3×10^{-2}	1×10^{-3}
	Mean	4×10^{-3}	1×10^{-2}	1×10^{-2}	2×10^{-2}	3×10^{-2}	5×10^{-2}	6×10^{-2}	6×10^{-2}	3×10^{-2}	3×10^{-4}
	S.I.R	6×10^{-3}	6×10^{-3}	6×10^{-3}	7×10^{-3}	8×10^{-3}	1×10^{-2}	1×10^{-2}	1×10^{-2}	1×10^{-2}	1×10^{-3}
	STD	1×10^{-3}	2×10^{-3}	3×10^{-3}	4×10^{-3}	4×10^{-3}	5×10^{-3}	6×10^{-3}	7×10^{-3}	5×10^{-3}	8×10^{-5}
2	Min	3×10^{-4}	8.7×10^{-5}	1×10^{-3}	2×10^{-3}	8×10^{-3}	2×10^{-2}	2×10^{-2}	2×10^{-2}	8×10^{-3}	6×10^{-6}
	Max	7×10^{-2}	8×10^{-2}	8×10^{-2}	8×10^{-2}	7×10^{-2}	7×10^{-2}	8×10^{-2}	1×10^{-1}	9×10^{-2}	1×10^{-2}
	MED	9×10^{-3}	1×10^{-2}	1×10^{-2}	2×10^{-2}	3×10^{-2}	4×10^{-2}	6×10^{-2}	6×10^{-2}	4×10^{-2}	1×10^{-4}
	Mean	7×10^{-3}	6×10^{-3}	1×10^{-2}	2×10^{-2}	3×10^{-2}	4×10^{-2}	6×10^{-2}	6×10^{-2}	3×10^{-2}	1×10^{-3}
	S.I.R	1×10^{-2}	1×10^{-2}	1×10^{-2}	1×10^{-2}	1×10^{-2}	1×10^{-2}	1×10^{-2}	1×10^{-2}	2×10^{-2}	2×10^{-3}
	STD	2×10^{-3}	6×10^{-3}	1×10^{-2}	1×10^{-2}	1×10^{-2}	1×10^{-2}	1×10^{-2}	1×10^{-2}	1×10^{-2}	6×10^{-4}
3	Min	1×10^{-5}	4×10^{-5}	2×10^{-3}	3×10^{-3}	1×10^{-2}	9×10^{-3}	6×10^{-3}	3×10^{-2}	1×10^{-2}	7×10^{-4}
	Max	7×10^{-2}	1×10^{-1}	1×10^{-1}	1×10^{-1}	1×10^{-1}	1×10^{-1}	1×10^{-1}	1×10^{-1}	1×10^{-1}	4×10^{-3}
	MED	9×10^{-3}	1×10^{-2}	2×10^{-2}	3×10^{-2}	5×10^{-2}	6×10^{-2}	7×10^{-2}	7×10^{-2}	5×10^{-2}	1×10^{-3}
	Mean	6×10^{-3}	5×10^{-3}	1×10^{-2}	2×10^{-2}	3×10^{-2}	5×10^{-2}	7×10^{-2}	8×10^{-2}	6×10^{-2}	1×10^{-3}
	S.I.R	1×10^{-2}	2×10^{-2}	2×10^{-2}	2×10^{-2}	2×10^{-2}	3×10^{-2}	2×10^{-2}	1×10^{-2}	1×10^{-2}	6×10^{-4}
	STD	2×10^{-3}	9×10^{-3}	1×10^{-2}	1×10^{-2}	2×10^{-2}	2×10^{-2}	1×10^{-2}	6×10^{-3}	1×10^{-2}	1×10^{-5}

For the convergence of FMWs-NN-PSOIPA, the global operators using the EVAF, ENSE, FIT, and TIC for 40 executions for the novel FOPSS are provided below in Table 2. It is noticeable that the Min global FIT, TIC, ENSE and EVAF values are found around 10^{-5}–10^{-7}, 10^{-5}–10^{-6}, 10^{-3}–10^{-4} and 10^{-2}–10^{-3}, whereas the S.I.R gages for these measures are found around 10^{-5}–10^{-7}, 10^{-7}–10^{-8}, 10^{-4}–10^{-5} and 10^{-2}–10^{-4} to solve the novel FOPSS. The classic global performance validates the clarity of FMWs-NN-PSOIPA.

Table 2. Global values through FMWs-NN-PSOIPA for solving the novel FOPSS.

Index	G.FIT		G.TIC		G.ENSE		G.EVAF	
	Min	SI.R	Min	SIR	MIN	SI.R	Min	SI.R
1	2.556×10^{-6}	2.285×10^{-5}	7.728×10^{-6}	2.673×10^{-7}	2.291×10^{-3}	3.330×10^{-5}	1.819×10^{-2}	2.636×10^{-2}
2	5.527×10^{-7}	3.006×10^{-5}	1.007×10^{-5}	3.272×10^{-7}	3.844×10^{-3}	6.650×10^{-5}	2.938×10^{-2}	5.920×10^{-4}
3	5.399×10^{-5}	7.898×10^{-7}	1.130×10^{-5}	3.491×10^{-8}	2.291×10^{-4}	3.330×10^{-4}	7.908×10^{-3}	7.100×10^{-2}

5. Conclusions

A novel design of the fractional order pantograph singular system using the applications of Meyer wavelets as a neural network is presented using the perceptions of standard forms of second-order singular and pantograph differential systems. The novel FOPSS is presented using the standard Lane–Emden equation and detailed discussions of the singularity, shape factor terms along with the fractional order forms. The singularity is noticed for a single time at $\eta = 0$, while the fractional terms appear twice as $\Re$ and $\Re + 1$. The perfection and exactness of the novel FOPSS is described using fractional Meyer wavelets as a neural network with the optimization procedures of global/local search procedures of the particle swarm optimization (PSO) and interior-point algorithm. The proposed FMWs-NN-PSOIPA is generally applied to solve the novel FOPSS to authenticate the stability, robustness, convergence and accuracy. To authenticate the correctness of the proposed FMWs-NN-PSOIPA, a comparison of the obtained outcomes with the true solutions is performed. The statistics using the operators TIC, Min, EVAF, S.I.R, Max, ENSE, Mean MED and STD are achieved using 40 executions to authenticate the consistency of the proposed FMWs-NN-PSOIPA. One can also prove that a variety of trials showed a greater accuracy level for the novel FOPSS. The novel FOPSS comprises pantographs, fractional terms and singular points, which shows the stiffness of the system and is considered complex to solve with conventional schemes. However, FMWs-NN-PSOIPA is an excellent choice to solve these types of intricate models.

In future, the FMWs-NN-PSOIPA can be implemented to solve fractional systems, nonlinear models and fluid systems [60–65].

Author Contributions: All authors have worked in the same way to reach the present results. Z.S. and J.L.G.G. lead the mathematical process while M.A.Z.R. and T.S. lead the validation process of the results. All authors have read and agreed to the published version of the manuscript.

Funding: This research has been partially supported by Ministerio de Ciencia, Innovacion y Universidades grant number PGC2018-0971-B-100 and Fundacion Seneca de la Region de Murcia grant number 20783/PI/18.

Institutional Review Board Statement: Not applicable.

Informed Consent Statement: Not applicable.

Conflicts of Interest: The authors declare no conflict of interest.

References

1. Sabir, Z.; Raja, M.A.Z.; Guirao, J.L.G.; Shoaib, M. A novel design of fractional Meyer wavelet neural networks with application to the nonlinear singular fractional Lane-Emden systems. *Alex. Eng. J.* **2021**, *60*, 2641–2659. [CrossRef]
2. Momani, S.; Ibrahim, R.W. On a fractional integral equation of periodic functions involving Weyl–Riesz operator in Banach algebras. *J. Math. Anal. Appl.* **2008**, *339*, 1210–1219. [CrossRef]
3. Bonilla, B.; Rivero, M.; Trujillo, J.J. On systems of linear fractional differential equations with constant coefficients. *Appl. Math. Comput.* **2007**, *187*, 68–78. [CrossRef]
4. Yu, F. Integrable coupling system of fractional soliton equation hierarchy. *Phys. Lett. A* **2009**, *373*, 3730–3733. [CrossRef]
5. Diethelm, K.; Ford, N.J. Analysis of fractional differential equations. *J. Math. Anal. Appl.* **2002**, *265*, 229–248. [CrossRef]
6. Diethelm, K.; Freed, A.D. On the solution of nonlinear fractional-order differential equations used in the modeling of viscoplasticity. In *Scientific Computing in Chemical Engineering II*; Springer: Berlin/Heidelberg, Germany, 1999; pp. 217–224.
7. Zhang, Y.; Sun, H.G.; Stowell, H.H.; Zayernouri, M.; Hansen, S.E. A review of applications of fractional calculus in Earth system dynamics. *Chaos Solitons Fractals* **2017**, *102*, 29–46. [CrossRef]
8. Evans, R.M.; Katugampola, U.N.; Edwards, D.A. Applications of fractional calculus in solving Abel-type integral equations: Surface–volume reaction problem. *Comput. Math. Appl.* **2017**, *73*, 1346–1362. [CrossRef]
9. Engheia, N. On the role of fractional calculus in electromagnetic theory. *IEEE Antennas Propag. Mag.* **1997**, *39*, 35–46. [CrossRef]
10. Daou, R.A.Z.; Samarani, F.E.; Yaacoub, C.; Moreau, X. Fractional Derivatives for Edge Detection: Application to Road Obstacles. In *Smart Cities Performability, Cognition, & Security*; Springer: Cham, Switzerland, 2020; pp. 115–137.
11. Torvik, P.J.; Bagley, R.L. On the appearance of the fractional derivative in the behavior of real materials. *J. Appl. Mech.* **1984**, *51*, 294–298. [CrossRef]
12. Aman, S.; Khan, I.; Ismail, Z.; Salleh, M.Z. Applications of fractional derivatives to nanofluids: Exact and numerical solutions. *Math. Model. Nat. Phenom.* **2018**, *13*, 2. [CrossRef]
13. Matlob, M.A.; Jamali, Y. The concepts and applications of fractional order differential calculus in modeling of viscoelastic systems: A primer. *Crit. Rev. Biomed. Eng.* **2019**, *47*, 249–276. [CrossRef]
14. Yang, X.J.; Machado, J.A.T.; Cattani, C.; Gao, F. On a fractal LC-electric circuit modeled by local fractional calculus. *Commun. Nonlinear Sci. Numer. Simul.* **2017**, *47*, 200–206. [CrossRef]
15. Sabir, Z.; Günerhan, H.; Guirao, J.L.G. On a new model based on third-order nonlinear multisingular functional differential equations. *Math. Probl. Eng.* **2020**, *2020*, 1683961. [CrossRef]
16. Abdelkawy, M.A.; Sabir, Z.; Guirao, J.L.G.; Saeed, T. Numerical investigations of a new singular second-order nonlinear coupled functional Lane–Emden model. *Open Phys.* **2020**, *18*, 770–778. [CrossRef]
17. Sabir, Z.; Sakar, M.G.; Yeskindirova, M.; Saldir, O. Numerical investigations to design a novel model based on the fifth order system of Emden–Fowler equations. *Theor. Appl. Mech. Lett.* **2020**, *10*, 333–342. [CrossRef]
18. Adel, W.; Sabir, Z. Solving a new design of nonlinear second-order Lane–Emden pantograph delay differential model via Bernoulli collocation method. *Eur. Phys. J. Plus* **2020**, *135*, 427. [CrossRef]
19. Sabir, Z.; Amin, F.; Pohl, D.; Guirao, J.L.G. Intelligence computing approach for solving second order system of Emden–Fowler model. *J. Intell. Fuzzy Syst.* **2020**, *38*, 7391–7406. [CrossRef]

20. Guirao, J.L.G.; Sabir, Z.; Saeed, T. Design and numerical solutions of a novel third-order nonlinear Emden–Fowler delay differential model. *Math. Probl. Eng.* **2020**, *2020*, 7359242. [CrossRef]
21. Sabir, Z.; Wahab, H.A.; Umar, M.; Sakar, M.G.; Raja, M.A.Z. Novel design of Morlet wavelet neural network for solving second order Lane-Emden equation. *Math. Comput. Simul.* **2020**, *172*, 1–14. [CrossRef]
22. Ockendon, J.R.; Tayler, A.B. The dynamics of a current collection system for an electric locomotive. *Proc. R. Soc. London A Math. Phys. Sci.* **1971**, *322*, 447–468.
23. Wake, G.C.; Cooper, S.; Kim, H.K.; Van-Brunt, B. Functional differential equations for cell-growth models with dispersion. *Commun. Appl. Anal.* **2000**, *4*, 561–574.
24. Bellen, A.; Guglielmi, N.; Torelli, L. Asymptotic stability properties of θ-methods for the pantograph equation. *Appl. Numer. Math.* **1997**, *24*, 279–293. [CrossRef]
25. Sinha, A.S.C. Stabilisation of time-varying infinite delay control systems. *IEE Proc. D-Control Theory Appl.* **1993**, *140*, 60–63. [CrossRef]
26. Ezz-Eldien, S.S.; Wang, Y.; Abdelkawy, M.A.; Zaky, M.A.; Aldraiweesh, A.A.; Machado, J.T. Chebyshev spectral methods for multi-order fractional neutral pantograph equations. *Nonlinear Dyn.* **2020**, *100*, 3785–3797. [CrossRef]
27. Ezz-Eldien, S.S. On solving systems of multi-pantograph equations via spectral tau method. *Appl. Math. Comput.* **2018**, *321*, 63–73. [CrossRef]
28. Anakira, N.R.; Jameel, A.; Alomari, A.K.; Saaban, A.; Almahameed, M.; Hashim, I. Approximate solutions of multi-pantograph type delay differential equations using multistage optimal homotopy asymptotic method. *J. Math. Fundam. Sci.* **2018**, *50*, 221–232. [CrossRef]
29. Isah, A.; Phang, C. A collocation method based on Genocchi operational matrix for solving Emden-Fowler equations. *J. Phys. Conf. Ser.* **2020**, *1489*, 012022. [CrossRef]
30. Yousefi, S.A.; Noei-Khorshidi, M.; Lotfi, A. Convergence analysis of least squares-Epsilon-Ritz algorithm for solving a general class of pantograph equations. *Kragujev. J. Math.* **2018**, *42*, 431–439. [CrossRef]
31. AŞI, Ş.Y.B.; Ismailov, N.A. Taylor operation method for solutions of generalized pantograph type delay differential equations. *Turk. J. Math.* **2018**, *42*, 395–406.
32. Sabir, Z.; Guirao, J.L.G.; Saeed, T. Solving a novel designed second order nonlinear Lane–Emden delay differential model using the heuristic techniques. *Appl. Soft Comput.* **2021**, *102*, 107105. [CrossRef]
33. Umar, M.; Sabir, Z.; Raja, M.A.Z.; Sánchez, Y.G. A stochastic numerical computing heuristic of SIR nonlinear model based on dengue fever. *Results Phys.* **2020**, *19*, 103585. [CrossRef]
34. Umar, M.; Sabir, Z.; Raja, M.A.Z. Intelligent computing for numerical treatment of nonlinear prey–predator models. *Appl. Soft Comput.* **2019**, *80*, 506–524. [CrossRef]
35. Sabir, Z.; Raja, M.A.Z.; Umar, M.; Shoaib, M. Neuro-swarm intelligent computing to solve the second-order singular functional differential model. *Eur. Phys. J. Plus* **2020**, *135*, 474. [CrossRef]
36. Sabir, Z.; Raja, M.A.Z.; Wahab, H.A.; Shoaib, M.; Gómez-Aguilar, J.F. Integrated neuro-evolution heuristic with sequential quadratic programming for second-order prediction differential models. *Numer. Methods Partial. Differ. Equ.* **2020**, 1–17. [CrossRef]
37. Raja, M.A.Z.; Mehmood, J.; Sabir, Z.; Nasab, A.K.; Manzar, M.A. Numerical solution of doubly singular nonlinear systems using neural networks-based integrated intelligent computing. *Neural Comput. Appl.* **2019**, *31*, 793–812. [CrossRef]
38. Sabir, Z.; Umar, M.; Guirao, J.L.G.; Shoaib, M.; Raja, M.A.Z. Integrated intelligent computing paradigm for nonlinear multi-singular third-order Emden–Fowler equation. *Neural Comput. Appl.* **2020**, *33*, 3417–3436. [CrossRef]
39. Umar, M.; Sabir, Z.; Raja, M.A.Z.; Shoaib, M.; Gupta, M.; Sánchez, Y.G. A Stochastic Intelligent Computing with Neuro-Evolution Heuristics for Nonlinear SITR System of Novel COVID-19 Dynamics. *Symmetry* **2020**, *12*, 1628. [CrossRef]
40. Raja, M.A.Z.; Umar, M.; Sabir, Z.; Khan, J.A.; Baleanu, D. A new stochastic computing paradigm for the dynamics of nonlinear singular heat conduction model of the human head. *Eur. Phys. J. Plus* **2018**, *133*, 364. [CrossRef]
41. Sabir, Z.; Raja, M.A.Z.; Le, D.N.; Aly, A.A. A neuro-swarming intelligent heuristic for second-order nonlinear Lane–Emden multi-pantograph delay differential system. *Complex Intell. Syst.* **2021**, 1–14. [CrossRef]
42. Sabir, Z.; Baleanu, D.; Raja, M.A.Z.; Guirao, J.L.G. Design of neuro-swarming heuristic solver for multi-pantograph singular delay differential equation. *Fractals* **2021**, *29*, 2140022. [CrossRef]
43. Sabir, Z.; Raja, M.A.Z.; Arbi, A.; Altamirano, G.C.; Cao, J. Neuro-swarms intelligent computing using Gudermannian kernel for solving a class of second order Lane-Emden singular nonlinear model. *AIMS Math* **2021**, *6*, 2468–2485. [CrossRef]
44. Khan, I.; Raja, M.A.Z.; Khan, M.A.R.; Shoaib, M.; Islam, S.; Shah, Z. Design of backpropagated intelligent networks for nonlinear second-order Lane–Emden pantograph delay differential systems. *Arab. J. Sci. Eng.* **2021**, 1–14. [CrossRef]
45. Nisar, K.; Sabir, Z.; Raja, M.A.Z.; Ibrahim, A.A.A.; Erdogan, F.; Haque, M.R.; Rodrigues, J.J.; Rawat, D.B. Design of Morlet Wavelet Neural Network for Solving a Class of Singular Pantograph Nonlinear Differential Models. *IEEE Access* **2021**, *9*, 77845–77862. [CrossRef]
46. Sabir, Z.; Raja, M.A.Z.; Kamal, A.; Guirao, J.L.G.; Le, D.-N.; Saeed, T.; Salama, M. Neuro-swarm heuristic unsign interior-point algorithm to solver a third kind of multi-singular nonlinear systems. *Math Biosci. Eng.* **2021**, *18*, 5285–5308. [CrossRef] [PubMed]

47. Nisar, K.; Sabir, Z.; Raja, M.A.Z.; Ibrahim, A.; Asri, A.; Rodrigues, J.J.P.C.; Khan, A.S.; Gupta, M.; Kamal, A.; Rawat, D.B. Evolutionary Integrated Heuristic with Gudermannian Neural Networks for Second Kind of Lane–Emden Nonlinear Singular Models. *Appl. Sci.* **2021**, *11*, 4725. [CrossRef]
48. Sabir, Z.; Nisar, K.; Raja, M.A.Z.; Ibrahim, A.A.B.A.; Rodrigues, J.J.; Al-Basyouni, K.S.; Mahmoud, S.R.; Rawat, D.B. Design of Morlet wavelet neural network for solving the higher order singular nonlinear differential equations. *Alex. Eng. J.* **2021**, *60*, 5935–5947. [CrossRef]
49. Rosca, D. Wavelet analysis on some surfaces of revolution via area preserving projection. *Appl. Comput. Harmon. Anal.* **2011**, *30*, 262–272. [CrossRef]
50. Muhammad, Y.; Khan, R.; Ullah, F.; Aslam, M.S.; Raja, M.A.Z. Design of fractional swarming strategy for solution of optimal reactive power dispatch. *Neural Comput. Appl.* **2020**, *32*, 10501–10518. [CrossRef]
51. Sharif, M.; Amin, J.; Raza, M.; Yasmin, M.; Satapathy, S.C. An integrated design of particle swarm optimization (PSO) with fusion of features for detection of brain tumor. *Pattern Recognit. Lett.* **2020**, *129*, 150–157. [CrossRef]
52. Tabibi, S.; Ghaffari, A. Energy-efficient routing mechanism for mobile sink in wireless sensor networks using particle swarm optimization algorithm. *Wirel. Pers. Commun.* **2019**, *104*, 199–216. [CrossRef]
53. Muhammad, Y.; Khan, R.; Raja, M.A.Z.; Ullah, F.; Chaudhary, N.I.; He, Y. Design of fractional swarm intelligent computing with entropy evolution for optimal power flow problems. *IEEE Access* **2020**, *8*, 111401–111419. [CrossRef]
54. Gao, H.; Zhang, K.; Yang, J.; Wu, F.; Liu, H. Applying improved particle swarm optimization for dynamic service composition focusing on quality of service evaluations under hybrid networks. *Int. J. Distrib. Sens. Netw.* **2018**, *14*, 1550147718761583. [CrossRef]
55. Wambacq, J.; Ulloa, J.; Lombaert, G.; François, S. Interior-point methods for the phase-field approach to brittle and ductile fracture. *Comput. Methods Appl. Mech. Eng.* **2021**, *375*, 113612. [CrossRef]
56. Huo, D.; le Blond, S.; Gu, C.; Wei, W.; Yu, D. Optimal operation of interconnected energy hubs by using decomposed hybrid particle swarm and interior-point approach. *Int. J. Electr. Power Energy Syst.* **2018**, *95*, 36–46. [CrossRef]
57. Raja, M.A.Z.; Ahmed, U.; Zameer, A.; Kiani, A.K.; Chaudhary, N.I. Bio-inspired heuristics hybrid with sequential quadratic programming and interior-point methods for reliable treatment of economic load dispatch problem. *Neural Comput. Appl.* **2019**, *31*, 447–475. [CrossRef]
58. Theodorakatos, N.P. A nonlinear well-determined model for power system observability using Interior-Point methods. *Measurement* **2020**, *152*, 107305. [CrossRef]
59. Raja, M.A.Z.; Shah, F.H.; Alaidarous, E.S.; Syam, M.I. Design of bio-inspired heuristic technique integrated with interior-point algorithm to analyze the dynamics of heartbeat model. *Appl. Soft Comput.* **2017**, *52*, 605–629. [CrossRef]
60. Dewasurendra, M.; Vajravelu, K. On the method of inverse mapping for solutions of coupled systems of nonlinear differential equations arising in nanofluid flow, heat and mass transfer. *Appl. Math. Nonlinear Sci.* **2018**, *3*, 1–14. [CrossRef]
61. Baskonus, H.M.; Bulut, H.; Sulaiman, T.A. New complex hyperbolic structures to the lonngren-wave equation by using sine-gordon expansion method. *Appl. Math. Nonlinear Sci.* **2019**, *4*, 129–138. [CrossRef]
62. İlhan, E.; Kıymaz, I.O. A generalization of truncated M-fractional derivative and applications to fractional differential equations. *Appl. Math. Nonlinear Sci.* **2020**, *5*, 171–188. [CrossRef]
63. Durur, H.; Tasbozan, O.; Kurt, A. New analytical solutions of conformable time fractional bad and good modified Boussinesq equations. *Appl. Math. Nonlinear Sci.* **2020**, *5*, 447–454. [CrossRef]
64. Baig, A.Q.; Naeem, M.; Gao, W. Revan and hyper-Revan indices of Octahedral and icosahedral networks. *Appl. Math. Nonlinear Sci.* **2018**, *3*, 33–40. [CrossRef]
65. Pandey, P.K. A new computational algorithm for the solution of second order initial value problems in ordinary differential equations. *Appl. Math. Nonlinear Sci.* **2018**, *3*, 167–174. [CrossRef]